A Connexin 40 Mutation Associated with a Malignant Variant of Progressive Familial Heart Block Type-1

Revised manuscript CIRCAE/2011/967604 (R2)

First author's surname: Makita

Short title: Connexin40 mutation in familial heart block

Naomasa Makita MD,PhD[1], Akiko Seki MD,PhD[2], Naokata Sumitomo MD,PhD[3], Halina Chkourko, MS[4], Shigetomo Fukuhara PhD[5], Hiroshi Watanabe MD,PhD[6], Wataru Shimizu MD,PhD[7], Connie R. Bezzina PhD[8], Can Hasdemir MD[9], Hideo Mugishima MD[3], Takeru Makiyama MD,PhD[10], Alban Baruteau MD[11], Estelle Baron BS[11], Minoru Horie MD,PhD[12], Nobuhisa Hagiwara MD,PhD[2], Arthur A.M. Wilde MD[8], Vincent Probst MD PhD[11], Hervé Le Marec MD[11], Dan M. Roden MD[13], Naoki Mochizuki MD,PhD[5], Jean-Jacques Schott PhD[11], Mario Delmar MD,PhD[4]

Department/Division of:

1. Molecular Physiology, Graduate School of Biomedical Sciences, Nagasaki University, Nagasaki, Japan
2. Cardiology, Tokyo Women's Medical University, Tokyo, Japan
3. Pediatrics and Child Health, Nihon University School of Medicine, Tokyo, Japan
4. Cardiology, New York University Medical School, New York, NY, USA.
5. Cell Biology, National Cerebral and Cardiovascular Center Research Institute, Suita, Japan
6. Cardiology, Niigata University Graduate School of Medical and Dental Sciences, Niigata, Japan

7. Cardiology, National Cerebral and Cardiovascular Center, Suita, Japan
8. Experimental Cardiology, Academic Medical Center, University of Amsterdam, Amsterdam, The Netherlands
9. Cardiology, Ege University School of Medicine, Bornova, Izmir, Turkey
10. Cardiovascular Medicine, Kyoto University Graduate School of Medicine, Kyoto, Japan
11. l'institut du thorax, INSERM UMR915, Nantes, France
12. Cardiovascular Medicine, Shiga University of Medical Science, Otsu, Japan
13. Pharmacology and Medicine, Vanderbilt University, Nashville, TN, USA

Address for correspondence:
Naomasa Makita MD,PhD
Department of Molecular Physiology,
Graduate School of Biomedical Sciences, Nagasaki University
1-12-4 Sakamoto, 852-8523 Nagasaki, Japan.
Phone: +81-95-819-7031, FAX: +81-95-819-7911
Email: makitan@nagasaki-u.ac.jp

Subject code:[132]Arrhythmias-basic studies

ABSTRACT

Background: Progressive familial heart block type I (PFHBI) is a hereditary arrhythmia characterized by progressive conduction disturbances in the His-Purkinje system. PFHBI has been linked to genes such as *SCN5A* that influence cardiac excitability, but not to genes that influence cell-to-cell communication. Our goal was to explore whether nucleotide substitutions in genes coding for connexin proteins would associate with clinical cases of PFHBI and if so, to establish a genotype-cell phenotype correlation for that mutation.

Methods and Results: We screened 156 probands afflicted with PFHBI. In addition to 12 sodium channel mutations, we found a germline *GJA5* (connexin40; Cx40) mutation (Q58L) in an afflicted family. Heterologous expression of Cx40-Q58L in connexin-deficient neuroblastoma cells resulted in marked reduction of junctional conductance (Cx40-WT: 22.2±1.7 nS, n=14; Cx40-Q58L: 0.56±0.34 nS, n=14; $p<0.001$) and diffuse localization of immunoreactive proteins in the vicinity of the plasma membrane without formation of gap junctions. Heteromeric co-transfection of Cx40-WT and Cx40-Q58L resulted in homogenous distribution of proteins in the plasma membrane rather than in membrane plaques in about 50% of cells; well-defined gap junctions were observed in other cells. Junctional conductance values correlated with

the distribution of gap junction plaques.

Conclusions: Mutation Cx40-Q58L impairs gap junction formation at cell-cell interfaces. This is the first demonstration of a germline mutation in a connexin gene that associates with inherited ventricular arrhythmias, and emphasizes the importance of Cx40 in normal propagation in the specialized conduction system.

Key Words: Heart block, Genes, Ion channels, Sudden death, Gap junctions

INTRODUCTION

Cardiac myocyte excitability in atria, His-Purkinje system and ventricles is largely determined by the properties of voltage-gated Na channels. Once activated, excitatory currents rapidly propagate to neighbouring cells via low-resistance intercellular channels called gap junctions, which facilitate the synchronous contraction of the heart.[1, 2] Loss of expression/function of cardiac gap junctions and/or sodium currents can severely impair action potential propagation, which sets the stage for life-threatening arrhythmias.[1, 2] Although multiple mutations in genes coding for components of the voltage-gated sodium channel complex have been previously described in relation to arrhythmias and sudden death in the young,[3] and connexin40 (Cx40) mutations have been implicated in atrial fibrillation,[4, 5] no study has identified an association between germ-line mutations in gap junction proteins and inherited ventricular arrhythmias in humans.

In this study, we investigated a group of patients diagnosed with “Progressive Familial Heart Block type I” (PFHBI, OMIM 113900), also known as progressive cardiac conduction defect (PCCD) or Lenégre-Lev disease[6, 7] is a dominant inherited disorder of the His-Purkinje system. Affected individuals show electrocardiographic evidence of bundle branch disease, i.e., right bundle branch block, left anterior or posterior

hemiblock, or complete heart block, with broad QRS complexes. The disease can progress from a normal electrocardiogram to right bundle branch block and from the latter to complete heart block. Affected individuals often present with family history of syncope, pacemaker implantation and/or sudden death.[8] While structural abnormalities have been invoked as cause of the disease,[6, 7] a number of cases present with normal cardiac structure and contractile function. Linkage analysis in a large South African PFHBI kindred[9] and a Lebanese kindred[10] mapped a causal locus on chromosome 19q13.3, and further work identified mutations in genes encoding for the "transient receptor potential non-selective cation channel, subfamily M, member 4 gene" (*TRPM4*)[11] at this locus. Haplo-insufficiency of *SCN5A* and aging have been implicated in PFHBI,[8] and age-dependent manifestations of the disease have been recapitulated in mice.[12]

Here, we sought to expand on the association between PFHBI, and mutations in genes relevant to action potential propagation; in particular, we assessed the possible association between nucleotide substitutions in connexin-coding genes, and PFHBI. We evaluated 156 probands of diverse ethnic backgrounds from Asia, Europe and North America with clinical diagnosis of PFHBI. In addition to sodium channel mutations previously reported,[13-15] we identified a germline

missense mutation in *GJA5* in a family with severe, early-onset disease. This gene codes for the gap junction protein connexin40 (Cx40), which predominantly expresses in atria and His-Purkinje system.[16] Heterologous expression experiments revealed that this novel mutation (Cx40-Q58L) significantly impaired the ability of Cx40 to form gap junction channels. Confocal microscopy showed that the Cx40-Q58L mutant but not the wild type (WT) failed to form plaques at sites of cell-cell apposition. Co-expression experiments indicated that Cx40-WT protein provided only partial rescue of the Cx40-Q58L cellular phenotype. This is the first description of a germline mutation in a connexin gene associated with inherited ventricular arrhythmias. Our results open the possibility of *GJA5* as a candidate gene for screening in PFHB1 patients; yet, in the absence of further evidence, screening may be limited to the research environment rather than include it as a part of the routine diagnostic examination[17]. Our data also emphasize the importance of Cx40 in the maintenance of normal propagation in the specialized conduction system of the human heart.

METHODS

Genetic screening of PFHB1

Genomic screening by PCR and DNA sequencing was performed for *GJA5* (Cx40), *GJA1* (Cx43), *GJC1* (Cx45), *KCNQ1*, *KCNH2*, *SCN5A*, *KCNE1*, *KCNE2, KCNJ2, SCN1B, SCN4B, HCN4.* (Primer information in online supplement.) All participating probands and family members gave written informed consent, in accordance with standards (Declaration of Helsinki) and local ethics committees.

Plasmid construction

A 1.1-kilobase Cx40-DNA fragment was subcloned into bicystronic plasmids pIRES2-EGFP and pIRES2-DsRED2. An EGFP or FLAG epitope was added at Cx40 C-terminal to generate EGFP- or FLAG-tagged Cx40. Site-directed mutagenesis (Q58L) was performed with QuikChange. Primer information and additional details in online supplement.

Cell culture and transfection

Constructs were introduced into connexin-deficient HeLa cells, or mouse neuroblastoma (N2A) cells using Lipofectamine as per manufacturer's protocol.

Electrophysiology

Gap junction currents were recorded from transiently-transfected N2A cell pairs using whole-cell double patch clamp techniques as previously described.[18, 19] Further details in online supplement.

Immunocytochemistry and Western blotting

HeLa cells, transfected with pEGFPN1-Cx40-WT, pCMV-FLAG-Cx40-Q58L, or both, were stained with anti-FLAG M2 antibody and Alexa546-labeled secondary antibody. EGFP and Alexa546 fluorescence images were recorded by confocal microscopy. For western blotting, N2A cells were transiently transfected with 3μg Cx40 plasmids. Two days after transfection, cells were lysed, proteins extracted and separated by conventional methods. Further details in online supplement.

Statistical analysis

Results are presented as mean±SEM. Mann-Whitney rank-sum tests with Bonferroni's post-hoc correction were used in comparisons for which normality or equal variance assumptions were invalid. In other instances, differences between groups were

assessed by one-way analysis of variance (ANOVA) followed by Bonferroni's post-hoc correction. Statistical significance was assumed for $P < 0.05$.

RESULTS

Genetic screening of PFHBI probands

We genetically screened 156 probands with clinical diagnosis of PFHBI. We identified 4 novel and 5 previously-reported mutations in *SCN5A,*[13, 15] 3 mutations in *SCN1B,*[14] and a novel germline heterozygous missense mutation in exon 2 of the Cx40 gene, *GJA5* (Supplemental Table S1). Mutations were not found in connexin genes *GJA1* (Cx43) or *GJC1* (Cx45) or in other genes screened (*KCNQ1, KCNH2, KCNE1, KCNE2, KCNJ2, HCN4* or *SCN4B*). Of the novel *SCN5A* mutations, one caused a modification of the amplitude and voltage gating kinetics of the sodium current in heterologously expressing cells (supplemental Figure S1); three other mutant constructs failed to express functional channels, suggesting that patients carrying the mutation were functionally haploinsuficient for Nav1.5 (supplemental Figure S1). The *GJA5* mutation (c. 173 A>T) caused an amino acid substitution (glutamine (Q) replaced by leucine (L)) at position 58 in Cx40 (Cx40-Q58L; Figures 1A-1B). The mutation was absent in 400 alleles from unaffected controls and in other 155 PFHBI probands. Screening of the entire gene panel (including *SCN5A* and *SCN1B*) revealed no other sequence modification in the DNA of this proband. Topological analysis placed amino acid 58 of Cx40 within the first extracellular loop (Figure 1C). The presence of glutamine

in this position is highly conserved among *GJA5* orthologs, and two other cardiac connexins, Cx43 and Cx45 (Figure 1D). The clinical and genotypic characteristics of proband and tested family members are described below.

Clinical phenotypes and genotype of the PFHBI pedigree with the *GJA5* mutation

The proband, an 11-year-old male at time of death, was first referred for evaluation when he was 6 years-old because of ECG abnormalities. Although asymptomatic at that time, his ECG showed advanced atrioventricular (AV) block, complete left bundle branch block (LBBB) and left axis deviation (Figure 2A). Echocardiography and cardiac scintigraphy did not reveal signs of structural heart disease. He experienced an episode of syncope at age 9; implantation of a permanent pacemaker was recommended by the physician but not authorized by the legal guardian. The proband died suddenly two years later during exercise (running) and the family declined postmortem examination. The proband's younger sister shares the Cx40-Q58L mutation. She is asymptomatic with a QRS duration at the upper limit of normal, left axis deviation that has been progressive (Supplemental Table S2) and QRS notch. These findings are consistent with impaired intraventricular conduction (Figure 2B). The mother died suddenly at age 30, after delivering the second child. An ECG on record,

obtained when she was 16 years old, was similar to that of the proband (compare Figure 2C with 2A). In addition, a ventricular tachycardia was recorded during the recovery phase of an exercise stress test (Supplemental Figure S2). DNA from the mother was not available for examination. Other family members, including proband's father, showed normal ECG. DNA analysis of proband's father and maternal grandparents revealed absence of the Cx40-Q58L mutation. Based on clinical data, and genotypic features of proband and sister, it is most likely that mutation Cx40-Q58L appeared *de novo* in the proband's mother. The data also indicate an early onset of PFHBI in this family, when compared to the natural history of the disease in most other cases.[8] As an initial step to assess the functional implications of mutation Cx40-Q58L, modified constructs were transiently expressed in an exogenous system and evaluated for localization and function.

Electrophysiological properties of mutant Cx40-Q58L channels

Connexin-deficient neuroblastoma (N2A) cells were transiently transfected with cDNA for Cx40-WT or Cx40-Q58L; electrophysiological properties of homologous Cx40 channels were analyzed by conventional dual whole-cell patch clamp. Figure 3A shows representative junctional current traces elicited by a transjunctional voltage gradient of

-60 mV. Average junctional conductance (Gj) decreased from 22.2±1.7 nS in Cx40-WT (n=14) to 0.56±0.34 nS in cells expressing the Cx40-Q58L mutant (n=14; $p<0.001$). The probability of functional coupling, calculated by dividing the number of electrically-coupled pairs by the number of pairs tested, was 100% and 57.1% for WT and Q58L, respectively.

Figure 3B depicts representative single channel recordings elicited by a transjunctional voltage of -60 mV in cell pairs expressing Cx40-WT or Cx40-Q58L. Unitary events for WT channels displayed current transitions corresponding to two conducting states (O_1 and O_2) of 43.3 pS and 119.5 pS, respectively. Figure 3C shows the event histograms for both cell types (Cx40-WT: N=3 cell pairs, n=303 events; Cx40-Q58L: N=3, n=416). The histogram for the Cx40-WT channels was best described by two Gaussian distributions centered at 136.2±2.3 pS and 53.1±5.3 pS. In contrast, the histogram for Cx40-Q58L channels was best described by a single Gaussian function, centered at 40.2±0.3 pS. Moreover, the length of time that a channel dwelled in the open state (dwell open time) was substantially longer for Cx40-Q58L than for WT channels (dwell open time for WT, 27.9±0.5 msec, N=4, n=186; for Q58L, 92.0±7.8 msec, N=3, n=163; Figure 3D). Of note, mutation Q58L had a strong dominant effect on formation of heterotypic functional gap junctions. Cells were transfected with either

pIRES2-EGFP-Cx40WT or pIRES2-DsRED2-Cx40Q58L, and heterotypic pairs identified by fluorescence microscopy (an EGFP-expressing cell paired with a DsRED2-expressing cell). We recorded from 8 cell pairs and detected unitary current events in only two pairs. A total of 57 events were recorded, and average macroscopic junctional conductance was 0.04±0.03 nS. Collectively, the data demonstrated that mutation Q58L significantly affects the biophysical properties of Cx40 channels and the overall ability of Cx40 gap junctions to form a low-resistance pathway between cells.

Electrophysiological properties and gap junction plaque formation in cells co-expressing WT and Q58L proteins.

In the clinical cases identified, mutation Q58L was detected only in one carrier allele. Therefore, we assessed the function of gap junctions in cells co-expressing WT and mutant proteins. N2A cells were co-transfected with cDNA for both GFP-tagged Cx40-WT and Cx40-Q58L (0.5 µg of pEGFPN1-Cx40-WT combined with 0.5 µg of pEGFPN1-Cx40- Q58L). Results were compared to those obtained when only one of the constructs (1 µg) was transfected. Cells expressing both constructs (WT/Q58L) showed intermediate conductance (15.4±3.7 nS, n=16) between WT (28.8±3.6 nS, n=16, $p<0.001$) and Q58L (0.28±0.11 nS, n=14, $p<0.001$; Figure 4A). These values

were comparable to those obtained using the bicistronic pIRES2-EGFP constructs (WT: 22.2±1.7 nS, n=14; WT/Q58L: 13.0±2.4 nS, n=17; Q58L: 0.56±0.34 nS, n=14). The co-expression results were consistent with those obtained using pIRES plasmids that tagged the cells both green and red, if co-transfected (Supplemental Figure S1). The probability of finding functional coupling in co-transfected cells was 76.5%, which was intermediate between WT (100%) and Q58L (57.1%).

The characteristics of gap junction plaques observed in cells co-expressing WT and Q58L varied significantly between pairs (Figure 4B). Nearly half of transfected (fluorescence-positive) cells exhibited clear and discrete gap junction plaques (arrow (a)) whereas the rest of fluorescent-positive cells showed diffuse expression pattern and absence of well-defined plaques (arrow (b)). Fluorescence-positive and gap junction plaque-positive cells were counted in 10 different views for each group, and efficacy of gap junction plaque formation was statistically analyzed (Figure 4C) by calculating the ratio of cells with gap junction plaques to the number of fluorescence-positive cells. In the Cx40-WT group, almost all fluorescent-positive cells exhibited clear gap junction plaques (94.9±1.9%, n=940), whereas there was a more diffuse and homogenous pattern with only occasional plaque formation in the Cx40-Q58L group (6.6±0.7%, n=1318, $p<0.001$ compared with WT). In contrast, results varied widely in cells

co-transfected with WT/Q58L; nearly half of fluorescence-positive cells exhibited gap junction plaques similar to those observed in cells transfected with the WT construct (48.2±2.4%, n=855, $p<0.001$), whereas the rest showed a diffuse expression pattern similar to that of Cx40-Q58L. To establish a better correlation between plaque formation and junctional conductance, both variables were measured concurrently in the same cell pair, for 39 N2A cell pairs where GFP-tagged plasmids of Cx40-WT and Cx40-Q58L were co-transfected. As shown in Figure 4D, about half of GFP-positive cell pairs showed a very small junctional conductance (<5 nS) and very few or negligible gap junction plaques (a). In the other half of cell pairs, small, dot-like junctional plaques correlated with intermediate junctional conductance (Gj) values (b), and there were clear, extensive gap junction plaques associated with Gj values larger than 25 nS (c). Overall, we found significant heterogeneity in the extent of electrical coupling, although the measurements of Gj correlated with the localization of proteins in transfected cells. These results indicate that the Q58L mutation significantly impairs the ability of cells to form gap junction plaques, though the effect is not purely dominant when both WT and mutant proteins are co-expressed.

Subcellular distribution of WT and Q58L Cx40 in transiently-transfected cells.

To further analyze the subcellular distribution of Cx40-WT and Cx40-Q58L proteins, the C-terminal of Cx40-WT was tagged with GFP, whereas the C-terminal of Cx40-Q58L was FLAG-tagged. After transfection of N2A cells with the tagged constructs, the distribution of each protein was examined by confocal microscopy. As shown in Figure 5, green color indicates the position of GFP-tagged molecules, whereas red indicates the position of FLAG-tagged molecules. In cells transfected only with GFP-tagged Cx40-WT, fluorescence was consistently detected at sites of cell-cell apposition, following the pattern previously described for GFP-labeled gap junction plaques (Figure 5A). A similar distribution was found when cells were transfected with FLAG-tagged Cx40-WT (not shown). In contrast, most FLAG-tagged Cx40-Q58L signal was evenly distributed around the cell, in the vicinity of the plasma membrane (Figure 5B). Biotinylation experiments showed that the Q58L mutation did not prevent the Cx40 protein from inserting into the membrane and presenting a domain reachable form the extracellular space (Supplemental Figure S2). Micoscopy experiments in cells co-expressing GFP-tagged Cx40-WT and FLAG-tagged Cx40-Q58L proteins yielded results intermediate to those obtained when only one construct was expressed. Nearly half of cell pairs showed both proteins distributed homogenously at or near the cell membrane, without formation of well-defined gap junction plaques (Figure 5C). These

images resembled those obtained when only Cx40-Q58L proteins were expressed (middle column of Figure 5B). In contrast, other cell pairs showed clustering of fluorescent signals within closely confined areas that appeared to be gap junction plaques (Figure 5D).

The experiments described above led us to speculate that the distribution and function of heteromeric connexons is determined by their mutant subunit content, whereby formation (or not) of plaques and channels are determined –at least in part- by the abundance of expression of one protein over the other. As an initial step to probe this hypothesis, we took advantage of the characteristics of the bicistronic plasmid pIRES, in which the expression rate of the upstream gene is several-fold greater than that of the downstream gene,[20] and explored the functional properties of heteromeric connexons. WT-Cx40 and GFP-tagged Q58L-Cx40 were subcloned into the pIRES vector, either alone or in combination, in the specific orientations shown in Figure 6A. Protein expression levels of WT-Cx40 and Q58L-Cx40 were determined by immunochemistry. In contrast to the data obtained when WT-Cx40 and GFP-tagged Q58L-Cx40 plasmids were co-transfected at a 1:1 ratio (lane 6), expression of heteromeric pIRES plasmids WT-IRES-Q58L-EGFP (lane 3) and

Q58L-EGFP-IRES-WT (lane 4) resulted in uneven protein expression levels of WT (40 kDa) and Q58L-EGFP (67 kDa), depending upon their orientation in the pIRES vector. Based on these observations, we constructed a homomeric WT-Cx40 plasmid (WT-IRES-WT) and heteromeric plasmids of WT-Cx40 and Q58L-Cx40 with different orientations (WT-IRES-Q58L and Q58L-IRES-WT; Figure 6B). Junctional conductance of cell pairs expressing WT-IRES-Q58L (25.3±2.8 nS, n=17) was nearly indistinguishable from that of the homomeric plasmid, WT-IRES-WT (27.8±1.4 nS, n=17, NS). By contrast, the converse heteromeric construct Q58L-IRES-WT showed substantially reduced junctional conductance (0.29±0.12 nS, n=15; $p<0.001$), comparable with that of the homomeric Q58L (0.56 ± 0.34 nS, Figure 3A). These results suggest that the final electrophysiological properties of the heteromeric connexons are determined predominantly by the numbers of mutant subunits in each gap junction, rather than defined by a dominant-negative effect.

DISCUSSION

Our genetic screening confirmed the association between *SCN5A* and *SCN1B* with PFHB1[13-15] and revealed novel mutations within these genes (supplemental Table S1). More importantly, we identified a particularly severe, early-onset case of PFHBI associated with a germline mutation in *GJA5* in two blood relatives (proband and sister) with clinical diagnosis of PFHBI. Our data also indicate that the protein expressed (Cx40-Q58L) failed to form functional gap junctions in an exogenous expression system and decreased the probability of gap junction formation in cells co-expressing the WT protein.

So far, *SCN5A*, *SCB1B* and *TRPM4* are the only genes associated with PFHB1[11, 13, 14]. The National Human Genome Research Institute database shows no association of *GJA5* SNPs to arrhythmias or conduction system diseases. PR interval and QRS have been associated with several loci including *SCN5A, SCN10A, NKX2.5, TBX5,* [21, 22] but not *GJA5* which is located at the chromosome 1q21.1. Overall, our results suggest that *GJA5* is a candidate gene associated with PFHBI, likely in a small fraction of the afflicted population. Yet, given the limited co-segregation observed in the reported family, we remain cautious in assigning a causative nature to the *GJA5*

mutation. It will be of great interest to expand the screening of *GJA5* at the research level to identify other cases associated with amino acid changes in Cx40, though it may be premature to include *GJA5* as a part of the routine diagnostic screen[17]. Our results also emphasize the importance of Cx40 in the maintenance of normal cardiac rhythm.

This is the first report of a germline mutation in Cx40 associated with a high risk of ventricular arrhythmias (Supplemental Figure S2). Other studies have shown somatic mutations of Cx40 or Cx43 in patients with idiopathic atrial fibrillation;[5, 23] those mutations were confined to the atria, and conduction abnormalities in the ventricles or His-Purkinje system were not observed. On the other hand, as in all cases involving identified genetic substrates for disease, the possibility of compound mutations in unexamined genes cannot be excluded. We do emphasize that the mutation led to a severe cellular phenotype in an exogenous expression system, supporting the argument that just the Q58L substitution can impair the formation of gap junctions, necessary for propagation of action potentials between cells.

Our results show that Cx40-Q58L was abundantly expressed in an exogenous system. The protein reached the vicinity of the cell membrane but failed to form gap junction plaques (Figure 5B). This result may be due to impaired docking of mutant

hemichannels within the intercellular space due to the mutation in the extracellular loop (Figure 1C). During trafficking, connexin subunits oligomerize to form a hemichannel (or "connexon"). Once at the site of cell contact, connexons from apposing cells dock, sealing the hydrophilic path (the channel pore) from the extracellular space. The locking of two connexons into one gap junction channel is thought to stabilize connexin subunits in place, facilitating aggregation of other oligomers into their vicinity, eventually forming a plaque. Amino acid substitutions within the extracellular loop, as in Q58L, can prevent hemichannel docking and thus plaque formation.[24] Our biotinylation experiments indicate that the Q58L protein integrates into the cell membrane, supporting the notion that the inability of mutant Q58L to form functional gap junctions is related to events that occur after the oligomer is delivered to the cell membrane, and before a functional dodecamer converts into a functional channel in a gap junction plaque.

Results obtained in cells co-expressing both mutant and WT proteins clearly show that one subunit can significantly influence the fate of the other (see Figure 5). This suggests that Cx40-Q58L subunits retain their ability to oligomerize, not only with other mutant subunits but also with the WT protein. Our results also present an interesting paradigm, in that neither the WT, nor the mutant construct exerted a dominant effect over the other. After transfection with equal amounts of cDNA, we found

cells where both WT and mutant proteins displayed the phenotype of the mutant construct, whereas in other cases, junctional plaques could be easily discerned (although an outline of the cell, likely resulting from the presence of the FLAG-tagged mutant protein, could still be observed; see red signal in Figure 5D). These results can be explained if we assume that the probability of proper targeting and integration of a connexon into a plaque decreases as a function of the number of mutant subunits contained. For co-transfection, we used equal amounts of cDNA. However, it is very likely that each cell was transfected with variable amounts of each construct and thus expressed variable amounts of each protein. We speculate that a majority (though of unknown stoichiometry) of WT connexin subunits are required in a connexon for proper formation of functional gap junctions. Thus, if a cell captures an abundance of Q58L cDNA, most oligomers will contain an excess of mutant subunits and gap junction formation will fail. If, on the other hand, that cell captures and expresses more of the WT cDNA, the distribution of the subunits within the oligomer will contain a majority of WT connexins and the connexon will be properly integrated into a channel. This hypothesis will require further testing, although data presented in Figure 6 support the concept that success or failure of functional channel formation may relate to relative abundance of each protein (WT or mutant). If our hypothesis is correct, it suggests that the distribution

of functional gap junctions in the His-Purkinje network of afflicted individuals could vary significantly among cells, depending on the extent of expression of each allele in each cell. The resulting phenotype may be that of a Purkinje network where gap junction-mediated coupling could be heterogeneous, setting the stage for local conduction block, micro-reentry and ventricular arrhythmias at the Purkinje network or at the Purkinje-muscle junction.[1, 2]

Overall, we show that both proband and sister have a genotype that a) is absent in hundreds of controls and in the unaffected parent (the father), b) disrupts an important functional domain of the protein, and c) disrupts the formation of gap junction channels. Our data therefore supports the notion of an association between the Cx40 mutation, and the clinical phenotype, and emphasizes the importance of future studies to assess the possible involvement of Cx40 mutations as causative of the disease.

ACKNOWLEDGMENTS

Authors thank Dr. A. L. George for critical reading, and Ms. M. Fukuoka and Ms. C.R. Ingram for technical assistance.

FUNDING SOURCES

Supported by research grant 21590921 (NM), Scientific Research B (Naoki Mochizuki), and Grant-in-Aid for Scientific Research on Innovative Areas (HD physiology) 22136007 (NM) from the Ministry of Education, Culture, Sports, Science and Technology, Japan, a Health and Labor Sciences Research Grant for research on measures for intractable diseases from the Ministry of Health (2010-145) (NM), Mitsubishi Pharma Research Foundation (NM), Japan-France Integrated Action Program (SAKURA) (NM, JJS), The Naito Foundation (NM, AS), Support Center for Women Health Care Professionals and Researchers (AS) 21590921, and grants GM057691, HL106632 and HL087226 from the National Institutes of Health (MD).

DISCLOSURES

None

REFERENCES

1. Saffitz JE, Lerner DL, Yamada KA. Gap junction distribution and regulation in the heart. In: Zipes DP, Jalife J, eds. *Cardiac Electrophysioohy: from cell to bedside*. Philadelphia: Saunders; 2004:181-191.

2. Park DS, Fishman GI. The cardiac conduction system. *Circulation*. 2011;123:904-915

3. Ruan Y, Liu N, Priori SG. Sodium channel mutations and arrhythmias. *Nat Rev Cardiol*. 2009;6:337-348

4. Firouzi M, Ramanna H, Kok B, Jongsma HJ, Koeleman BPC, Doevendans PA, Groenewegen WA, Hauer RNW. Association of human connexin40 gene polymorphisms with atrial vulnerability as a risk factor for idiopathic atrial fibrillation. *Circ. Res.* 2004;95:e29-33

5. Gollob MH, Jones DL, Krahn AD, Danis L, Gong X-Q, Shao Q, Liu X, Veinot JP, Tang ASL, Stewart AFR, Tesson F, Klein GJ, Yee R, Skanes AC, Guiraudon GM, Ebihara L, Bai D. Somatic mutations in the connexin 40 gene (GJA5) in atrial fibrillation. *N. Engl. J. Med.* 2006;354:2677-2688

6. Lenegre J. Etiology and pathology of bilateral bundle branch block in relation to

complete heart block. *Prog. Cardiovasc. Dis.* 1964;6:409-444

7. Lev M, Kinare SG, Pick A. The pathogenesis of atrioventricular block in coronary disease. *Circulation*. 1970;42:409-425

8. Probst V, Kyndt F, Potet F, Trochu JN, Mialet G, Demolombe S, Schott JJ, Baro I, Escande D, Le Marec H. Haploinsufficiency in combination with aging causes SCN5A-linked hereditary Lenegre disease. *J. Am. Coll. Cardiol.* 2003;41:643-652

9. Brink PA, Ferreira A, Moolman JC, Weymar HW, van der Merwe P-L, Corfield VA. Gene for progressive familial heart block type I maps to chromosome 19q13. *Circulation*. 1995;91:1633-1640

10. de Meeus A, Stephan E, Debrus S, Jean M-K, Loiselet J, Weissenbach J, Demaille J, Bouvagnet P. An isolated cardiac conduction disease maps to chromosome 19q. *Circ. Res.* 1995;77:735-740

11. Kruse M, Schulze-Bahr E, Corfield V, Beckmann A, Stallmeyer B, Kurtbay G, Ohmert I, Schulze-Bahr E, Brink P, Pongs O. Impaired endocytosis of the ion channel TRPM4 is associated with human progressive familial heart block type I. *J. Clin. Invest.* 2009;119:2737-2744

12. Royer A, van Veen TAB, Le Bouter S, Marionneau C, Griol-Charhbili V, Leoni A-L,

Steenman M, van Rijen HVM, Demolombe S, Goddard CA, Richer C, Escoubet B, Jarry-Guichard T, Colledge WH, Gros D, de Bakker JMT, Grace AA, Escande D, Charpentier F. Mouse model of SCN5A-linked hereditary Lenegre's disease. Age-related conduction slowing and myocardial fibrosis. *Circulation*. 2005;111:1738-1746

13. Schott JJ, Alshinawi C, Kyndt F, Probst V, Hoorntje TM, Hulsbeek M, Wilde AA, Escande D, Mannens MM, Le Marec H. Cardiac conduction defects associate with mutations in SCN5A. *Nat. Genet.* 1999;23:20-21

14. Watanabe H, Koopmann TT, Le Scouarnec S, Yang T, Ingram CR, Schott JJ, Demolombe S, Probst V, Anselme F, Escande D, Wiesfeld AC, Pfeufer A, Kaab S, Wichmann HE, Hasdemir C, Aizawa Y, Wilde AA, Roden DM, Bezzina CR. Sodium channel beta1 subunit mutations associated with Brugada syndrome and cardiac conduction disease in humans. *J. Clin. Invest.* 2008;118:2260-2268

15. McNair WP, Ku L, Taylor MRG, Fain PR, Dao D, Wolfel E, Mestroni L, the Familial Cardiomyopathy Registry Research Group. SCN5A mutation associated with dilated cardiomyopathy, conduction disorder, and arrhythmia. *Circulation*. 2004;110:2163-2167

16. Miquerol L, Meysen S, Mangoni M, Bois P, van Rijen HVM, Abran P, Jongsma H,

Nargeot J, Gros D. Architectural and functional asymmetry of the His-Purkinje system of the murine heart. *Cardiovasc. Res.* 2004;63:77-86

17. Ackerman MJ, Priori SG, Willems S, Berul C, Brugada R, Calkins H, Camm AJ, Ellinor PT, Gollob M, Hamilton R, Hershberger RE, Judge DP, Le Marec H, McKenna WJ, Schulze-Bahr E, Semsarian C, Towbin JA, Watkins H, Wilde A, Wolpert C, Zipes DP. HRS/EHRA expert consensus statement on the state of genetic testing for the channelopathies and cardiomyopathies. *Heart Rhythm*. 2011;8:1308-1339

18. Seki A, Coombs W, Taffet SM, Delmar M. Loss of electrical communication, but not plaque formation, after mutations in the cytoplasmic loop of connexin43. *Heart Rhythm*. 2004;1:227-233

19. Anumonwo JMB, Taffet SM, Gu H, Chanson M, Moreno AP, Delmar M. The carboxyl terminal domain regulates the unitary conductance and voltage dependence of connexin40 gap junction channels. *Circ. Res.* 2001;88:666-673

20. Bochkov YA, Palmenberg AC. Translational efficiency of EMCV IRES in bicistronic vectors is dependent upon IRES sequence and gene location. *Biotechniques*. 2006;41:283-284

21. Holm H, Gudbjartsson DF, Arnar DO, Thorleifsson G, Thorgeirsson G,

Stefansdottir H, Gudjonsson SA, Jonasdottir A, Mathiesen EB, Njolstad I, Nyrnes A, Wilsgaard T, Hald EM, Hveem K, Stoltenberg C, Lochen M-L, Kong A, Thorsteinsdottir U, Stefansson K. Several common variants modulate heart rate, PR interval and QRS duration. *Nat. Genet.* 2010;42:117-122

22. Pfeufer A, van Noord C, Marciante KD, Arking DE, Larson MG, Smith AV, Tarasov KV, Muller M, Sotoodehnia N, Sinner MF, Verwoert GC, Li M, Kao WHL, Kottgen A, Coresh J, Bis JC, Psaty BM, Rice K, Rotter JI, Rivadeneira F, Hofman A, Kors JA, Stricker BHC, Uitterlinden AG, van Duijn CM, Beckmann BM, Sauter W, Gieger C, Lubitz SA, Newton-Cheh C, Wang TJ, Magnani JW, Schnabel RB, Chung MK, Barnard J, Smith JD, Van Wagoner DR, Vasan RS, Aspelund T, Eiriksdottir G, Harris TB, Launer LJ, Najjar SS, Lakatta E, Schlessinger D, Uda M, Abecasis GR, Muller-Myhsok B, Ehret GB, Boerwinkle E, Chakravarti A, Soliman EZ, Lunetta KL, Perz S, Wichmann HE, Meitinger T, Levy D, Gudnason V, Ellinor PT, Sanna S, Kaab S, Witteman JCM, Alonso A, Benjamin EJ, Heckbert SR. Genome-wide association study of PR interval. *Nat. Genet.* 2010;42:153-159

23. Thibodeau IL, Xu J, Li Q, Liu G, Lam K, Veinot JP, Birnie DH, Jones DL, Krahn AD, Lemery R, Nicholson BJ, Gollob MH. Paradigm of genetic mosaicism and lone atrial fibrillation: Physiological characterization of a connexin 43-deletion

mutant identified from atrial tissue. *Circulation*. 2010;122:236-244

24. Sosinsky GE, Nicholson BJ. Structural organization of gap junction channels. *Biochim. Biophys. Acta*. 2005;1711:99-125

FIGURE LEGENDS

Figure 1. *GJA5* mutation identified in a family with the clinical diagnosis of PFHB1.

A**:** Family pedigree. Genetically affected and unaffected individuals shown with closed and open symbols, respectively. Hatched circle: Proband's mother not genotyped; clinical data suggest she was a *de novo* mutation carrier. Number below each symbol: age at registration or age of sudden death (parenthesis). B: Sequence electropherogram of exon 2 *GJA5* of proband. Arrow indicates heterozygous missense mutation of leucine (CTG) for glutamine-58 (CAG). C: Cx40 predicted membrane topology indicating position Q58 in first extracellular loop. D: Sequence alignment of human Cx40 and its homologues (residues 45-70). Notice also conservation in human Cx43 and Cx45. Dashes indicate residues identical with the top sequence.

Figure 2. ECGs of proband and affected family members. A: ECG of proband at age 6 showing advanced AV block, complete LBBB and left axis deviation. Patient died suddenly five years later. B: ECG of proband's sister at age 6 showing QRS duration at upper limit of normal, left axis deviation that has been progressive, and QRS notch in V4 and V5 (arrows) consistent with impaired intraventricular conduction. C: ECG of proband's mother at age 16 showing complete LBBB and left axis deviation. She died

suddenly at age 30.

Figure 3. Whole-cell and single channel properties of Cx40-WT and Cx40-Q58L channels. A: Voltage pulse (top) and junctional current (bottom) from a homomeric WT cell pair (left; Gj=12.9 nS) and a Q58L cell pair (right; Gj=1.2 nS). B: Unitary currents recorded from homomeric Cx40-WT (upper) and Cx40-Q58L (lower) channels. O_1 and O_2 refer to two conducting (open) unitary levels of current. C: All-event histograms pooled from WT (left; N=3) and Q58L (right; N=3) cells with homologous channels. WT: Gaussian peaks centered at 136.2±2.3 pS and 53.1±5.3 pS. Q58L: Best fit by a single Gaussian distribution centered at 40.2±0.3 pS (N=3). D: Frequency of events in relation to dwell open time. Binned data were fit by single exponentials. τ_{open}: WT=27.9±0.5 msec, N=4 cells, n=186 events; Q58L= 92.0±7.8 msec, N=3 cells, n=163 events).

Figure 4. Macroscopic conductance and gap junction plaque morphology in cells co-expressing Cx40-WT and Cx40-Q58L. A: Junctional conductance of cells transfected with plasmid pEGFPN1-Cx40-WT (1 µg; data labeled “WT”), pEGFPN1-Cx40-Q58L (1 µg; column “Q58L”), or co-transfected with WT and Q58L (WT/Q58L: pEGFPN1-Cx40-WT 0.5µg+ pEGFPN1-Cx40-Q58L 0.5 µg). Asterisks:

p<0.001 compared with WT. B: Phase contrast/fluorescence overlay image of N2A cells transfected with WT/Q58L constructs. Arrow “a” points to gap junction plaque; arrow “b” shows example of cells transfected but void of gap junction plaque. Calibration bar: 20 µm. C: Efficacy of gap junction plaque formation was measured as ratio between number of gap junction plaque-positive cells and number of fluorescent-positive cells (WT: n=940, WT/Q58L: n=855, Q58L: n=1,318). Asterisks: p<0.001 compared with WT. D: Representative images of phase contrast (left), EGFP fluorescence (middle), and junctional conductance (right) from N2A cells co-transfected with pEGFPN1-Cx40-WT (0.25 µg) and pEGFPN1-Cx40-Q58L (0.25 µg). Three different examples (a-c) are shown to illustrate relation between plaque morphology and recorded junctional conductance.

Figure 5. Subcellular distribution of Cx40-WT and Cx40-Q58L in transiently transfected cells. HeLa cells were transiently transfected with pEFGPN1-Cx40-WT (3.0 µg; panels A), pCMV-FLAG-Cx40-Q58L (3.0 µg; panels B) or pEFGPN1-Cx40-WT (1.5 µg) plus pCMV-FLAG-Cx40-Q58L (1.5 µg; panels C), immunostained for the respective tag protein and visualized by confocal laser scanning microscopy. Notice gap junction plaques (A) absent in Q58L transfectants (B) and present in some (D) but not all

(C) co-transfected cells. Bars: 20 μm.

Figure 6. Mutant subunit abundance correlated with gap junction function. A: N2A cells were transiently transfected with 3 μg Cx40 constructs in IRES plasmids (see below). Cell lysates were analyzed by Western blot using anti-Cx40 (upper panel) and anti-GAPDH antibodies (lower panel). The number in each lane corresponds to plasmid noted below. Samples from cells co-transfected with plasmids 1 and 2 (1.5 μg each) were loaded on lane 6. Double bands of WT-Cx40 (40 kDa) and Q58L-EGFP (67 kDa) are shown in lanes 3,4, 6,7. Results were repeated in three separate experiments. Overexposure (lane 7) confirmed expression of the high molecular weight protein in lane 3. B: Junctional conductance of homomeric and heteromeric constructs (WT-IRES-Q58L and Q58L-IRES-WT). Conductance of cell pairs expressing WT-IRES-WT (n=17) was comparable to heteromeric constructs WT-IRES-Q58L (n=17). However, converse heteromeric construct Q58L-IRES-WT (n=15) showed significantly reduced conductance ($p<0.001$ vs. WT-IRES-WT and WT-IRES-Q58L). *** and NS indicate $p<0.001$ and no statistical significance, respectively.

Figure 1

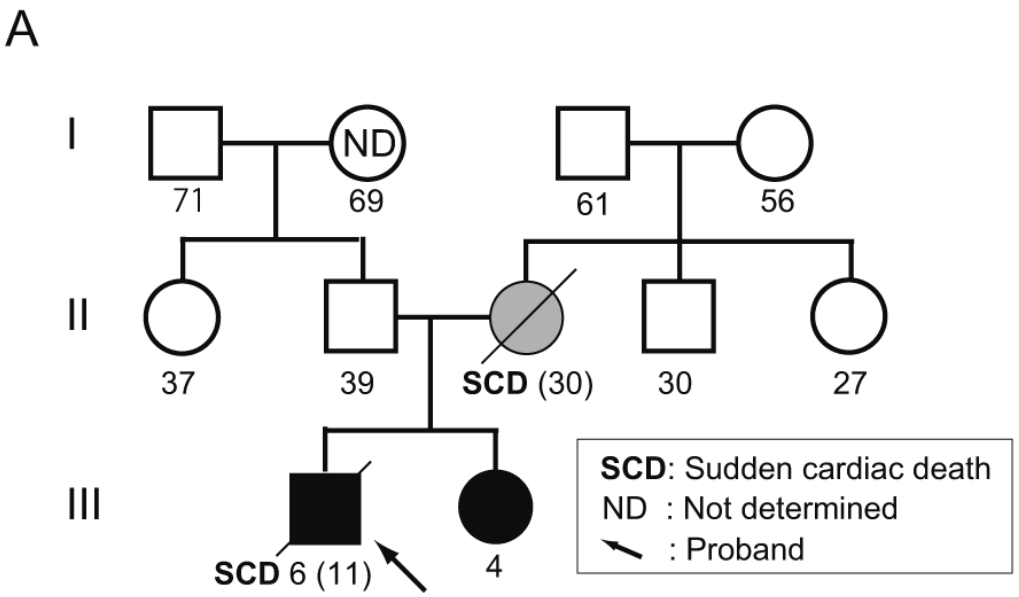

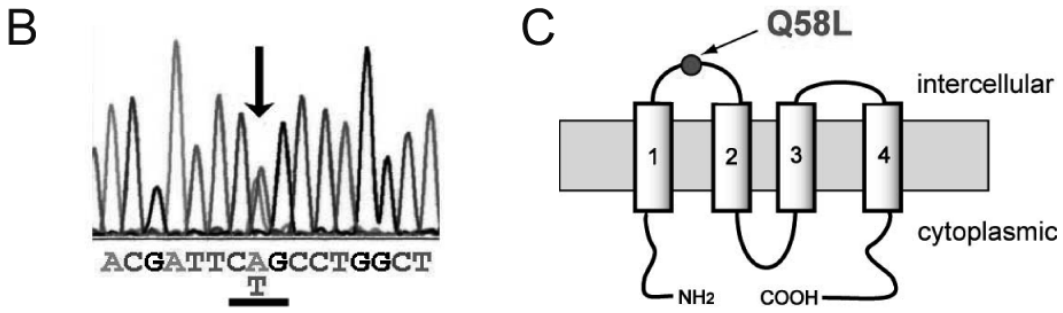

D

```
                          45                  58                  70
                          |                   |                   |
Human Cx40                WGDEQADFRCDTIQPGCQNVCYDQAF
Chimpanzee                ----------------------------
Mouse                     ----------------------------
Rat                       ----------------------------
Dog                       --------Q---M----G---------
Bovine                    --------L---M----E---------
Chicken                   -----S--M---Q----E-----K--
Zebra fish(cx45.6)        -----S--M---L----T-----R--
Zebra fish(cx41.8)        -----E--T---E----E-----R-

Human Cx43                -----SA---N-Q----E-----KS-
Human Cx45                FE---FE-V-N-L----RQT---R--
```

Figure 2


A
I
aVR
V1
V4
II
aVL
V2
V5
III
aVF
V3
V6
V1
100 Hz
25.0 mm/s
10.0 mm/mV
marquette electronics, inc.
Jupiter, Florida
12SL tm
v250
B
C

Figure 3

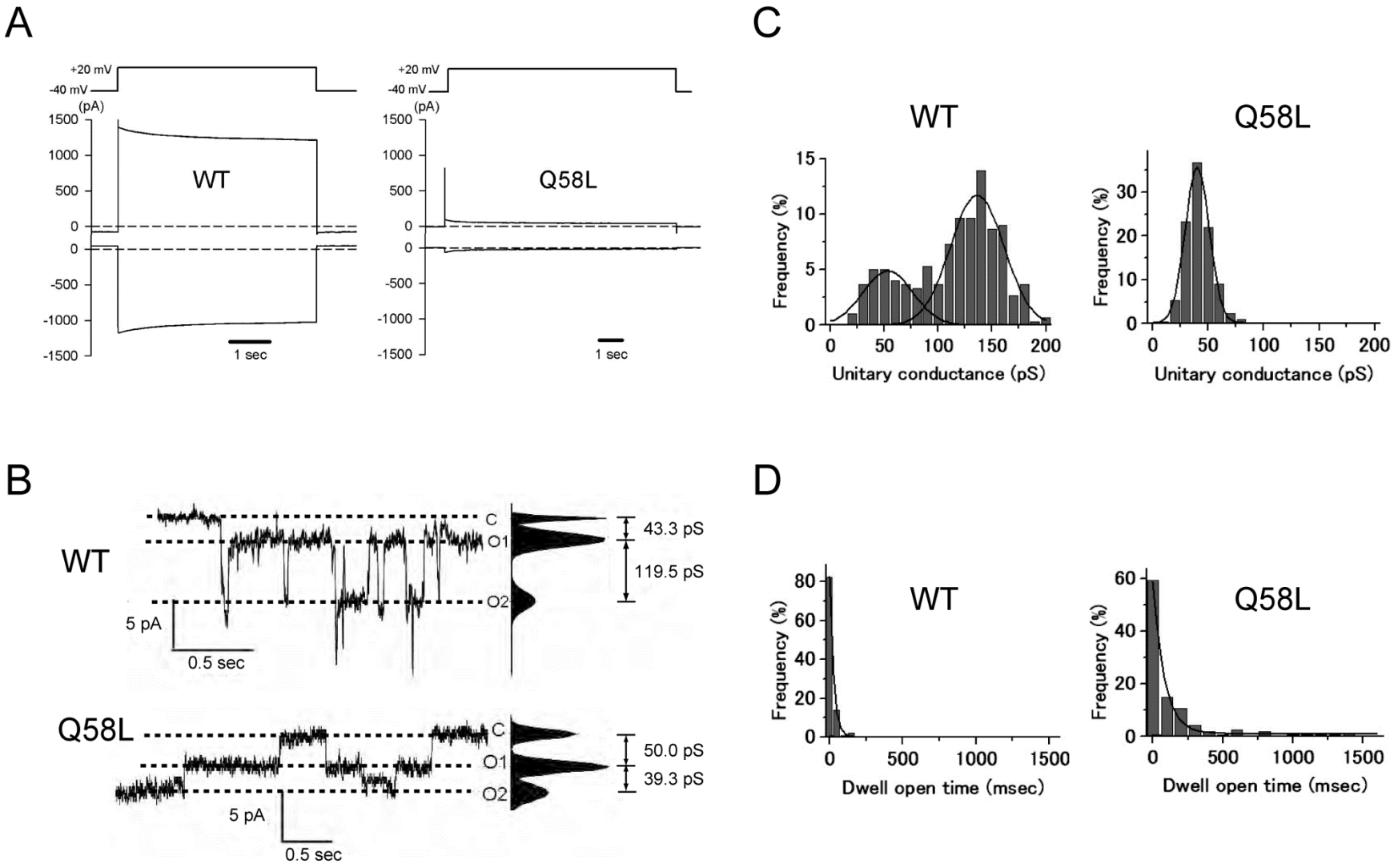
A
+20 mV
-40 mV
(pA)
1500
1000
500
0
-500
-1000
-1500
WT
Q58L
1 sec
B
WT
C
O1
O2
43.3 pS
119.5 pS
5 pA
0.5 sec
Q58L
50.0 pS
39.3 pS
C
WT
Q58L
Frequency (%)
Unitary conductance (pS)
D
Dwell open time (msec)

Figure 4

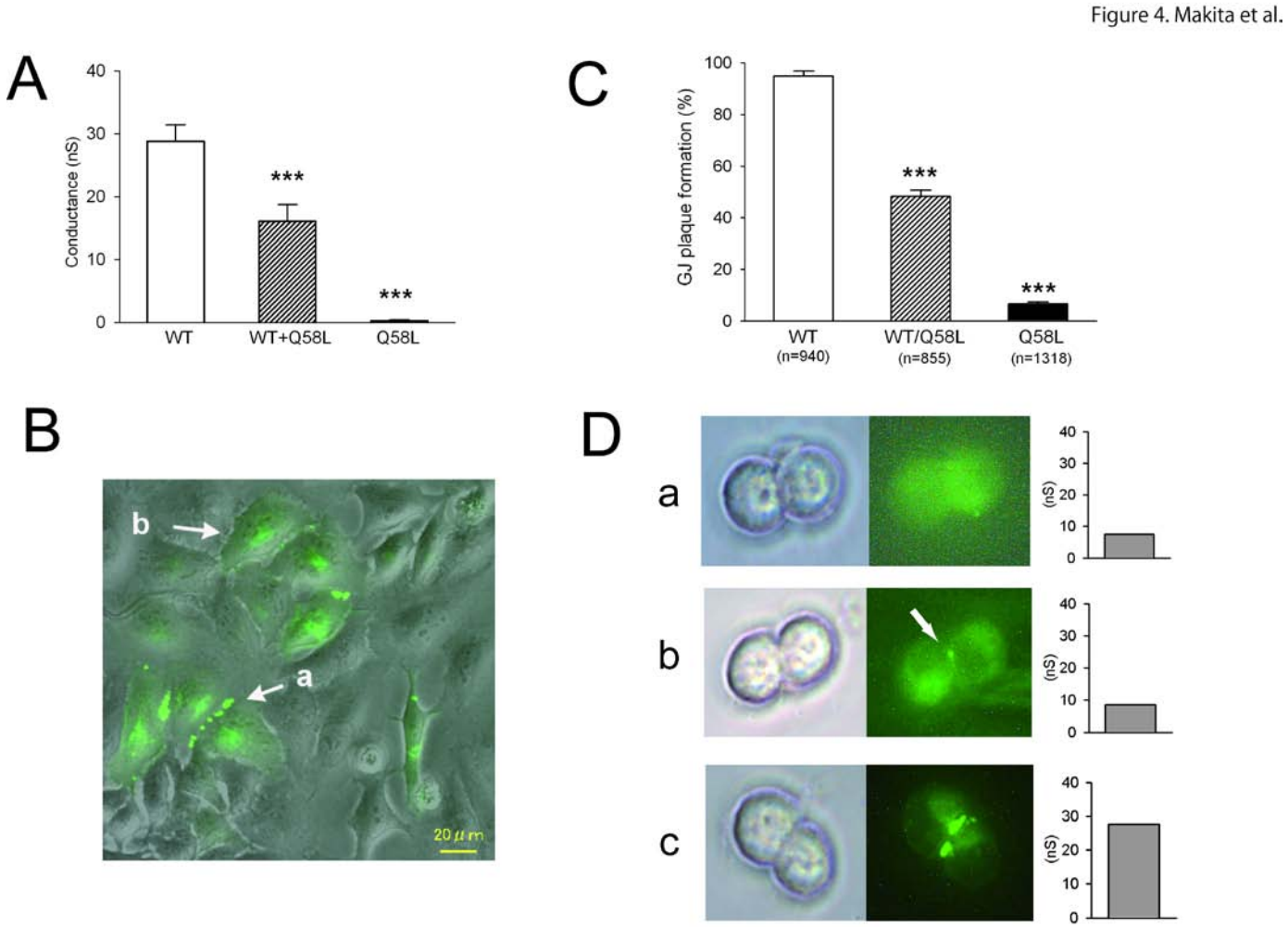
Figure 4. Makita et al.
A
Conductance (nS)
40
30
20
10
0
***
***
WT
WT+Q58L
Q58L
C
GJ plaque formation (%)
100
80
60
40
20
0
***
***
WT
(n=940)
WT/Q58L
(n=855)
Q58L
(n=1318)
B
b
a
20 μm
D
a
b
c
40
30
20
10
0
(nS)

Figure 5

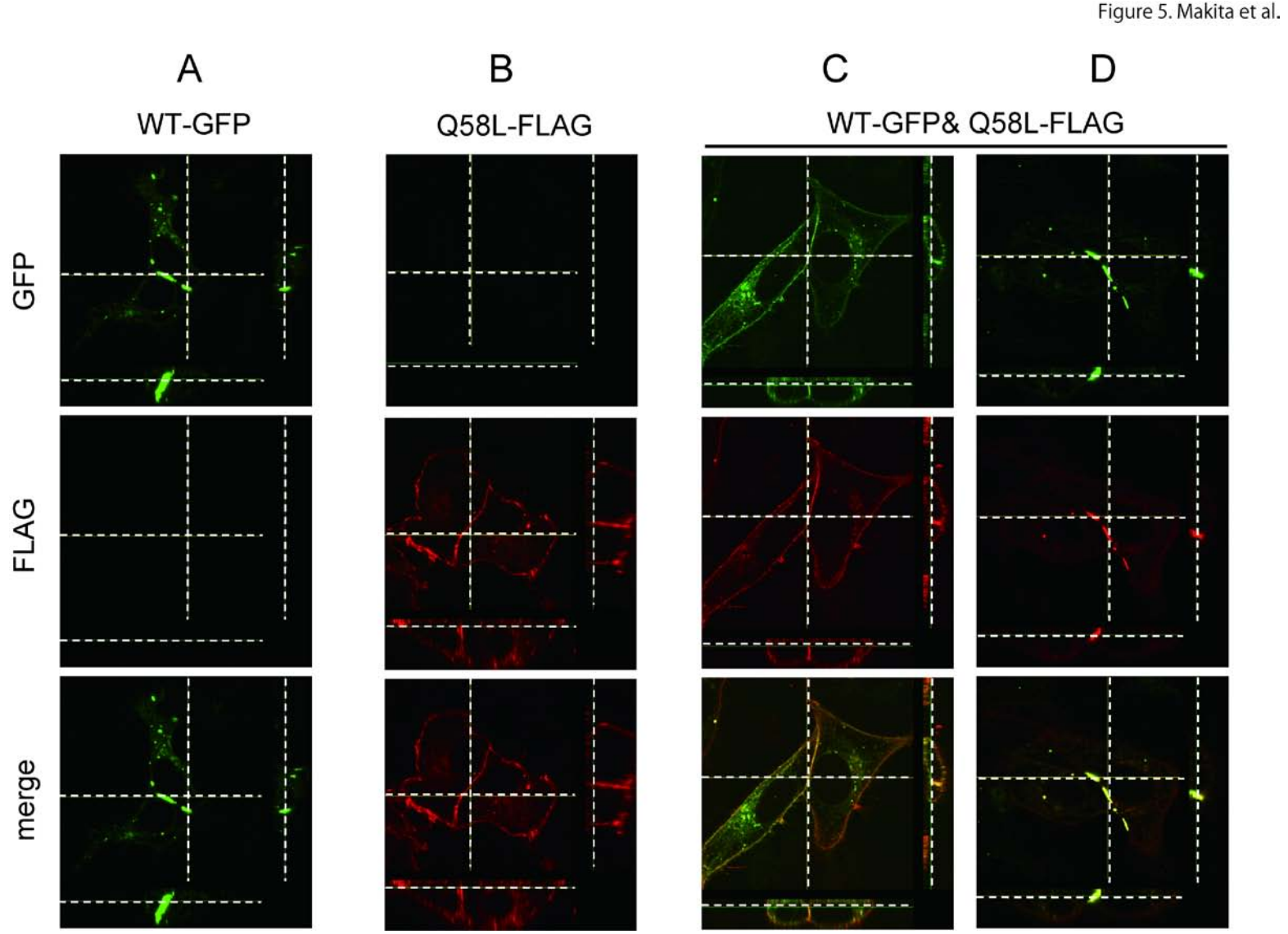
Figure 5. Makita et al.
A
B
C
D
WT-GFP
Q58L-FLAG
WT-GFP& Q58L-FLAG
GFP
FLAG
merge

Figure 6

Figure 6. Makita et al.

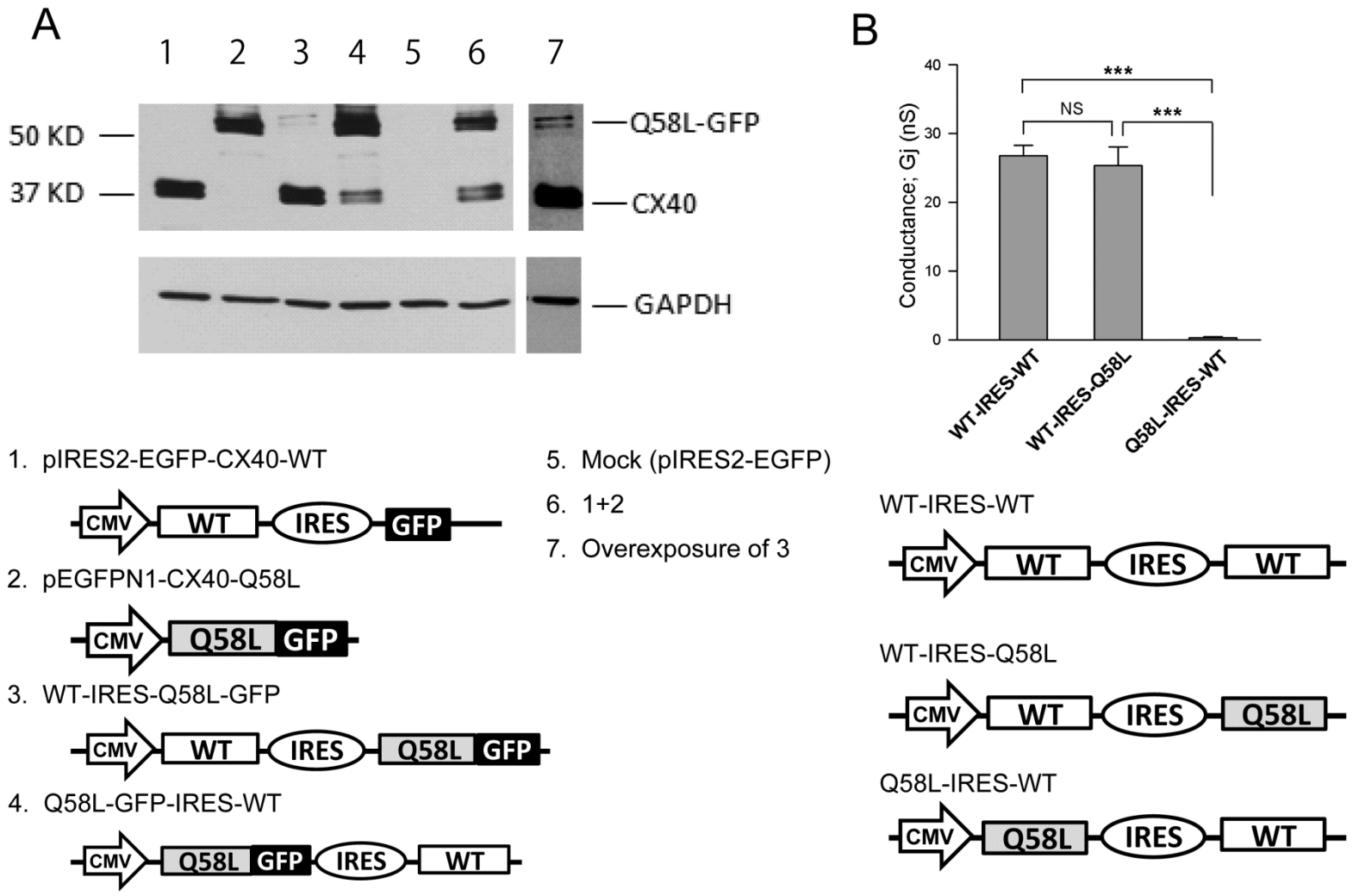

SUPPLEMENTAL MATERIAL

SUPPLEMENTAL METHODS

1. Genetic screening of PFHB1

The exon 2 of *GJA5* and exon 3 of *GJC1* that cover the entire coding region of the Cx40 and Cx45, respectively, were amplified by PCR from genome DNA using following primer sets.

GJA5	Forward (Cx40-F2)	5’-TGGAATCCCAGAACATGATAGA-3’
	Reverse (Cx40-R2)	5’-TCAGTTCAGAAGGGACACGTCT-3’
GJC1	Forward (Cx45-F1)	5'-GAGCCACCCTACCCAACTGA-3'
	Reverse (Cx45-R1)	5'-ACCAGAGCCAAATGTTTACTCAA -3'

The coding regions of *KCNQ1*, *KCNH2*, *SCN5A*, *KCNE1*, *KCNE2*, *KCNJ2*, *SCN1B*, *SCN4B*, *HCN4*, *GJA1* (Cx43) were amplified by PCR using exon flanking intronic primers as previously described.[1-8] Direct DNA sequencing was performed using ABI 3130 genetic analyzer (Applied Biosystems).

2. Plasmid construction

A 1.1-kilobase DNA fragment, encompassing the entire coding region of Cx40, was amplified by PCR from human genomic DNA using the following primers.

Forward (Cx40-F7)	5’-GAAGATCTCACCATGGGCGATTGGAGC TTCCT-3’
Reverse (Cx40-R2X)	5’-GGAATTCACACTGATAGGTCATCTG-3’

(Underlines represent the restriction recognition sequences for BglII and EcoRI, respectively)

The PCR fragment was digested with BglII/EcoRI and subcloned into a bicystronic plasmid pIRES2-EGFP or pIRES2-DsRED2 (Takara Bio), for visual identification of cells expressing

connexins and green (EGFP) or red fluorescent protein (DsRED2), respectively. Site-directed mutagenesis was performed by QuikChange (Stratagene) as per manufacturer's instructions. Sequences of PCR-amplified regions were verified for both strands. For EGFP-tagged Cx40 plasmid, the1.1 kb coding sequence of WT and Q58L Cx40 were PCR-amplified by the following primers.

Forward (Cx40-F2X) 5'-AACAAGCTTCACCATGGGCGATTGGAGCTTCCT-3'

Reverse (Cx40-R5X) 5'-GCGGATCCACTGATAGGTCATCTGA-3'

(Underlines represent the restriction recognition sequences for HindIII and BamHI, respectively.) The PCR fragment was digested with HindIII/BamHI and subcloned in frame into the plasmid pEGFP-N1 (Takara Bio), generating fusion constructs (pEGFPN1-Cx40-WT and pEGFPN1-Cx40-Q58L). FLAG-tagged Cx40 plasmids were constructed by replacing the 0.8 kb EGFP fragment of the pEGFPN1-Cx40 plasmids in frame with the FLAG epitope (DYKDDDDK) cDNA at the C-terminal of the Cx40 (pCMV-FLAG-Cx40-WT and pCMV-FLAG-Cx40-Q58L, respectively. EGFP-tag or FLAG-tag did not change the conductance or the gating properties of Cx40 (data not shown).

Bicistronic constructs of WT-Cx40 and Q58L-Cx40 were made using the plasmid pIRES (Takara Bio). The WT-Cx40 (1.1 kb) and EGFP-tagged Q58L-Cx40 (1.8kb) were subcloned either at the upstream or the downstream cloning sites of the IRES (internal ribosomal entry site) (Fig 6B, constructs 3 and 4). Homomeric WT-Cx40 construct and the heteromeric constructs (WT-IRES-Q58L and Q58L-IRES-WT) in Fig 6C were constructed by PCR. WT-Cx40 or Q58L-Cx40 cDNAs were initially PCR-amplified by the primers Cx40-Fa and Cx40-Rb, and the PCR products were digested with NheI/EcoRI and subcloned in the upper multiple cloning sites NheI/EcoRI of pIRES.

Forward (Cx40-Fa) 5'-GCGCTAGCCACCATGGGCGATTGGAGC TTCCT-3'

Reverse (Cx40-Rb) 5’-AGAATTCTCACACTGATAGGTCATCTG-3’

(Underlines represent the restriction recognition sequences for NheI and EcoRI, respectively)

Similarly, WT-Cx40 or Q58L-Cx40 cDNAs were PCR-amplified by the primers Cx40-F8 and Cx40-R3, and the PCR products were digested with XbaI/NotI and subcloned in the lower multiple cloning sites XbaI/NotI of pIRES.

Forward (Cx40-F8) 5’-GCTCTAGACACCATGGGCGATTGGAGC TTCCT-3’

Reverse (Cx40-R3) 5’-ATAAGATGCGGCCGCTCACACTGATAGGTCATCTG-3’

(Underlines represent the restriction recognition sequences for XbaI and NotI, respectively)

Translation rate of the upstream cloned gene is generally greater than that cloned at the downstream site. Expression levels of WT-Cx40 (40 kDa) and Q58L-Cx40-GFP (67 kDa) are determined by western blotting using ant-Cx40 antibody.

3. **Cell culture and transfection**

Connexin 40 constructs were introduced into connexin-deficient HeLa cells or mouse neuroblastoma (N2A) cells, maintained in F-12 or Minimum Essential Medium, respectively, supplemented with 10% fetal bovine serum. HeLa and N2A cells were transfected with plasmids using Lipofectamine LTX or Lipofectamine 2000 (Invitrogen) as per the manufacturer’s protocol.

4. Electrophysiology

Gap junction currents from heterologously expressed N2A cell pairs were recorded using whole-cell double patch clamp techniques as previously described.[9, 10] Recordings were carried out independently in each cell of a pair using two Axopatch 200B amplifiers (Axon Instruments). Current signals were filtered at 100-200 Hz and digitally sampled at 1-2 KHz

using an analog-to-digital interface (Digidata 1322A, Axon Instruments). The data were analyzed using Clampfit 9.2 (Axon Instruments) and Origin 7.5 (Origin Lab). The external solution contained (in mmol/L) 160 NaCl, 10 CsCl, 2 $CaCl_2$, 0.6 $MgCl_2$ and 10 HEPES, at pH 7.4. The intracellular (pipette) solution contained (in mmol/L) 130 $CsCl_2$, 0.5 $CaCl_2$, 10 HEPES, 10 EGTA, 2 Na_2ATP and 3 MgATP (added daily), (pH = 7.2). Pipette resistance was 5-10 MΩ. Octanol was added directly to the external solution at the final concentration of 1 mmol/L at each experiment. Experiments were carried out at room temperature (20-22 ºC). All the chemicals were purchased from Sigma or Wako (Tokyo, Japan).

Gap junction channel conductance (g_j) was determined by conventional methods. Briefly, both cells in the pair ($cell_1$ and $cell_2$) were independently voltage-clamped at the same holding potential (-40 mV). $Cell_1$ was then stepped to a new voltage, thus creating a potential difference across the junction (V_j). The current in $cell_2$ was considered equal and opposite to the junctional current (I_j), and g_j was measured from the ratio I_j/V_j. The pulses were 2 or 5 sec in duration with an interpulse interval of 15 sec. Unitary conductance was obtained from pairs where only one or two functional channels were spontaneously detected. In some cases, cells were uncoupled by exposure to 1 mmol/L octanol. Histograms of events were obtained from channels recorded during repetitive 10-20 sec steps to V_j= +60 mV. To measure unitary conductance, only junctional current traces with events that lasted for longer than 20 ms were included. [9, 10] All-points histograms of digitized current traces and the frequency distribution histograms were constructed using Origin 7.5.

To analyze the electrophysiological properties of heterotypic gap junctions consisting of Cx40-WT and Cx40-Q58L, N2A cells were transiently transfected with either Cx40-WT (pIRES2-EGFP plasmid) or Cx40-Q58L (pIRES2-DsRED2 plasmid). Sixteen hours later, both cells were split with trypsin/EDTA and co-cultured. On the following day, the

heterotypic cell pairs of Cx40-WT (green) and Cx40-Q58L (red) were visually identified under fluorescent microscopy. Experiments were carried out at room temperature (20-22 ºC).

5. Immunocytochemistry

HeLa cells were cultured on a glass-bottom dish (Asahi Techno Glass, Chiba, Japan) and transfected with the fusion plasmids of pEGFPN1-Cx40-WT, pCMV-FLAG-Cx40-Q58L, or both. Next day, the cells were washed with phosphate-buffered saline (PBS), fixed in PBS containing 2% formaldehyde for 30 min at 4 °C, and permeabilized with 0.05% Triton X-100 for 30 min at 4 °C. After blocking with PBS containing 4% bovine serum albumin for 1 h at room temperature, the cells were stained with anti-FLAG M2 antibody (mouse monoclonal, 1:200, Sigma) for 1 h at room temperature. Protein reacting with antibody was visualized with Alexa 546-labeled secondary antibody (goat, 1:300, Invitrogen). EGFP and Alexa 546 fluorescence images were recorded with a FluoView FV1000 confocal microscope (Olympus Co, Tokyo) with a 60x oil immersion objective.

6. Western blotting

N2A cells maintained in a 6 well dish were transiently transfected with 3 μg Cx40 plasmids. Two days after transfection, cells were washed with PBS, and total cell lysate was extracted with lysis buffer including 50 mM Tris (pH7.5), 150 mM NaCl, 1% TritonX-100, 0.1 μg/ml aprotinin, 1x complete protease inhibitor (Roche Applied Science). Lysates precleared by centrifugation at 15,000 xg for 10 min were subjected to SDS-PAGE and immunoblotting with rabbit anti-Cx40 antibody (Millipore). Proteins reacting with primary antibodies were visualized by ECL system (GE Healthcare). The membrane was reprobed by anti-GAPDH antibody (Sigma).

7. Surface biotinylation

HeLa cells plated on 100 mm dishes were transiently transfected with 11 μg of pEGFPN1-Cx40-Q58L using Lipofectamine 2000 (Invitrogen). Surface biotinylation was performed 48 hours after transfection using the Pierce Cell Surface Protein Isolation Kit (Thermo Scientific, #89881) as per the manufacturer's protocol. Briefly, after 30 min of biotin labeling reaction at 4 °C, cell were lysed, mixed with NeutrAvidin agarose, and loaded on a column. The biotinylated proteins were eluted with the elution buffer. Fractions of the flowthrough, elute, and input lysate (1:1 diluted with lysate buffer) were subjected to a 4-12% gradient SDS-PAGE and immunobotting with anti-Cx40 antibodies (Cx40-A, 1:50 dilution, Alpha Diagnostic International). Proteins reacting with primary antibodies were visualized by LI-COR infrared imaging technology. Detection was done using anti-rabbit IRDye 800CW (1:10,000) antibodies (LI-COR Biosciences, # 926-32213).

8. Functional evaluation of novel *SCN5A* mutations associated with PFHB1

Three novel *SCN5A* mutations associated with PFHB1 were identified; a missense mutation F777L, a compound heterozygous frame shift mutation p.P701fsX710 plus p.P2006fsX2037, and a frame shift mutation pV1764fsX1786. These mutations were not found in 400 unaffected control alleles. Functional properties of these mutations were evaluated by whole-cell patch clamp. The mammalian expression plasmids encoding the mutations were constructed by site-directed mutagenesis as we described previously using a human Na channel α subunit (Nav1.5) cDNA.[11] The human cell line tsA-201 was transiently transfected together with Na channel β1 subunit, and the whole-cell Na currents were recorded as we previously described.[11] Electrode resistance ranged from 0.8 to 1.5 MΩ. Data

acquisition was carried out using an Axopatch 200B patch clamp amplifier and pCLAMP10 software (Axon Instruments). Currents were filtered at 5 kHz (–3 dB; 4-pole Bessel filter) and digitized using an analog-to-digital interface (Digidata 1440A; Axon Instruments). Experiments were carried out at room temperature (20–22°C). Voltage errors were minimized using series resistance compensation (generally 80%). Cancellation of the capacitance transients and leak subtraction were performed using an online P/4 protocol. The pulse protocol cycle time was 10 s. The data were analyzed using Clampfit 10 (Axon Instruments) and SigmaPlot 11 (SPSS Science). The holding potential was –120 mV. The bath solution contained (in mmol/l): 145 NaCl, 4 KCl, 1.8 $CaCl_2$, 1 $MgCl_2$, 10 HEPES, and 10 glucose, pH 7.35 (adjusted with NaOH). The pipette solution (intracellular solution) contained (in mmol/l): 10 NaF, 110 CsF, 20 CsCl, 10 EGTA, and 10 HEPES, pH 7.35 (adjusted with CsOH). The time from establishing the whole-cell configuration to onset of recording was consistent cell-to-cell to exclude the possible time-dependent shift of steady-state inactivation. To determine activation parameters, the current-voltage relationship was fit to the Boltzmann equation $I = (V - V_{rev}) \times G_{max} \times (1 + \exp[V - V_{1/2}] / k)^{-1}$, where I is the peak Na current during the test pulse potential V. The parameters estimated by the fitting are V_{rev} (reversal potential), G_{max} (maximum conductance), and k (slope factor) (Supplemental Figure 1B). Steady-state availability for fast inactivation was measured with a standard double-pulse protocol (Supplemental Figure 1C, left inset), and the data were fit with the Boltzmann equation $I/I\text{max} = (1 + \exp[(V - V_{1/2}) / k])^{-1}$, where I_{max} is the maximum peak Na current, to determine the membrane potential for $V_{1/2}$ and k. Functional properties of other mutations in *SCN5A* or *SCN1B* were previous reported (Supplemental table S1).

SUPPLEMENTAL FIGURE LEGEND

Supplemental Figure S1

Functional properties of the novel *SCN5A* mutations

Panel A shows whole-cell Na currents recorded from tsA201cells expressing wild type (WT) Nav1.5 (left) or Nav1.5 mutant F777L (right). Currents were elicited by step pulses from -90 mV to +60 mV (10 mV step) from a holding potential of -120 mV. Bars: 5 msec and 2 nA. Non-inactivated late currents were not observed. Panel B shows current-voltage relationship. Average peak current density was significantly reduced in F777L ($p<0.001$). WT: 391.7±47.1 pA/pF, n=15 (open circles). F777L: 301.2±30.0 pA/pF, n=9 (closed circles). Panel C shows that the voltage-dependence of activation of F777L channels (closed circles) was not different from control, whereas steady-state inactivation curve was significantly shifted in the hyperpolarizing direction in F777L (WT: $V_{1/2}$= -87.1±0.5 mV, n=25; F777L: $V_{1/2}$= -92.4 ± 1.3 mV, n=9; $p<0.001$). These biophysical properties suggest a decrease in the number of functional (conductive) sodium channels during the action potential upstroke consequent to the mutation. Previous studies have revealed that mutations A1180V[12] and D1275N[13], also found in our series (see supplemental Table S1), exhibit minor functional abnormalities when expressed in cultured cells, though more drastic changes are observed when the channels are expressed in cardiomyocytes[14]. Cells expressing compound heterozygous mutations p.P701fsX710 and p.P2006fsX2037, or a frame shift mutation pV1764fsX1786, exhibited no Na current, suggesting haploinsufficiency of cardiac Na current in the afflicted population.

Supplemental Figure S2

Exercise stress test of the proband's mother

Electrocardiographic recording obtained from the probands's mother during a treadmill exercise stress test at the age of 16. A heart rate of 177 bpm was achieved after 9 min 20 sec of exercise test by Bruce protocol. During the recovery phase at 1 min 17 sec, superior axis narrow QRS ventricular tachycardia with a rate of 110 bpm was observed (upper panel) .Ventricular tachycardia was spontaneously terminated at 20 min 23 sec of the recovery phase (lower panel).

Supplemental Figure S3

Co-expression of Cx40-WT and Cx40-Q58L in N2A cells.

Panels A-C show fluorescence images from a cell pair recorded from cells co-transfected with pIRES2-EGFP-Cx40-WT and pIRES2-DsRED2-Cx40-Q58L (0.5 μg each). Notice expression of both the green (A) and the red marker (B), giving a yellow color in the overlay (C). Calibration bar: 20 μm. Panel D: Junctional conductance recorded from cell pairs as that shown in panels A-C was 18.9±5.4 nS (n=6). This number was not statistically different from that obtained from pairs expressing WT-GFP and Q58L-GFP (average Gj= 13.0±2.4 nS; n=17).

Supplemental Figure S4

Surface biotinylation of Q58L-Cx40 expressed in HeLa cells.

HeLa cells transfected with pEGFPN1-Cx40-Q58L were surface-labeled with biotin, and lysed. Cell lysate was mixed with NeutrAvidin agarose and loaded on a column. Flowthough, elute (biotin-labeled membrane fraction) and the input lysate (1:1 diluted with lysate buffer) were subjected to SDS-PAGE and immunoblotting. A single 67KDa band of similar intensity

was detected in both elute and the input lysate, but not in the flowthrough. These data indicate that mutation Q58L did not prevent surface expression of the Cx40 protein.

SUPPLEMENTAL REFERENCES

1. Wang Q, Li Z, Shen J, Keating MT. Genomic organization of the human SCN5A gene encoding the cardiac sodium channel. *Genomics*. 1996;34:9-16
2. Splawski I, Shen J, Timothy KW, Lehmann MH, Priori S, Robinson JL, Moss AJ, Schwartz PJ, Towbin JA, Vincent GM, Keating MT. Spectrum of mutations in long-QT syndrome genes. KVLQT1, HERG, SCN5A, KCNE1, and KCNE2. *Circulation*. 2000;102:1178-1185
3. Plaster NM, Tawil R, Tristani-Firouzi M, Canun S, Bendahhou S, Tsunoda A, Donaldson MR, Iannaccone ST, Brunt E, Barohn R, Clark J, Deymeer F, George AL, Jr., Fish FA, Hahn A, Nitu A, Ozdemir C, Serdaroglu P, Subramony SH, Wolfe G, Fu YH, Ptacek LJ. Mutations in Kir2.1 cause the developmental and episodic electrical phenotypes of Andersen's syndrome. *Cell*. 2001;105:511-519.
4. Makita N, Sloan-Brown K, Weghuis DO, Ropers HH, George AL, Jr. Genomic organization and chromosomal assignment of the human voltage-gated Na^+ channel beta 1 subunit gene (SCN1B). *Genomics*. 1994;23:628-634
5. Watanabe H, Koopmann TT, Le Scouarnec S, Yang T, Ingram CR, Schott JJ, Demolombe S, Probst V, Anselme F, Escande D, Wiesfeld AC, Pfeufer A, Kaab S, Wichmann HE, Hasdemir C, Aizawa Y, Wilde AA, Roden DM, Bezzina CR. Sodium channel beta1 subunit mutations associated with Brugada syndrome and cardiac conduction disease in humans. *J. Clin. Invest.* 2008;118:2260-2268
6. Medeiros-Domingo A, Kaku T, Tester DJ, Iturralde-Torres P, Itty A, Ye B, Valdivia C, Ueda K, Canizales-Quinteros S, Tusie-Luna MT, Makielski JC, Ackerman MJ. *SCN4B*-encoded sodium channel β4 subunit in congenital long-QT syndrome. *Circulation*. 2007;116:134-142

7. Schulze-Bahr E, Neu A, Friederich P, Kaupp UB, Breithardt G, Pongs O, Isbrandt D. Pacemaker channel dysfunction in a patient with sinus node disease. *J. Clin. Invest.* 2003;111:1537-1545

8. Britz-Cunningham SH, Shah MM, Zuppan CW, Fletcher WH. Mutations of the connexin43 gap-junction gene in patients with heart malformations and defects of laterality. *New Engl. J. Med.* 1995;332:1323-1330

9. Seki A, Coombs W, Taffet SM, Delmar M. Loss of electrical communication, but not plaque formation, after mutations in the cytoplasmic loop of connexin43. *Heart Rhythm*. 2004;1:227-233

10. Anumonwo JMB, Taffet SM, Gu H, Chanson M, Moreno AP, Delmar M. The carboxyl terminal domain regulates the unitary conductance and voltage dependence of connexin40 gap junction channels. *Circ. Res.* 2001;88:666-673

11. Makita N, Behr E, Shimizu W, Horie M, Sunami A, Crotti L, Schulze-Bahr E, Fukuhara S, Mochizuki N, Makiyama T, Itoh H, Christiansen M, McKeown P, Miyamoto K, Kamakura S, Tsutsui H, Schwartz PJ, George AL, Roden DM. The E1784K mutation in SCN5A is associated with mixed clinical phenotype of type 3 long QT syndrome. *J. Clin. Invest.* 2008;118:2219-2229

12. Ge J, Sun A, Paajanen V, Wang S, Su C, Yang Z, Li Y, Wang S, Jia J, Wang K, Zou Y, Gao L, Wang K, Fan Z. Molecular and clinical characterization of a novel SCN5A mutation associated with atrioventricular block and dilated cardiomyopathy. *Circ Arrhythmia Electrophysiol*. 2008;1:83-92

13. Groenewegen WA, Firouzi M, Bezzina CR, Vliex S, van Langen IM, Sandkuijl L, Smits JP, Hulsbeek M, Rook MB, Jongsma HJ, Wilde AA. A cardiac sodium channel mutation cosegregates with a rare connexin40 genotype in familial atrial standstill.

Circ. Res. 2003;92:14-22

14. Watanabe H, Nogami A, Ohkubo K, Kawata H, Hayashi Y, Ishikawa T, Makiyama T, Nagao S, Yagihara N, Takehara N, Kawamura Y, Sato A, Okamura K, Hosaka Y, Sato M, Fukae S, Chinushi M, Oda H, Okabe M, Kimura A, Maemura K, Watanabe I, Kamakura S, Horie M, Aizawa Y, Shimizu W, Makita N. Electrocardiographic Characteristics and SCN5A Mutations in Idiopathic Ventricular Fibrillation Associated with Early Repolarization. *Circulation: Arrhythmia and Electrophysiology*. 2011

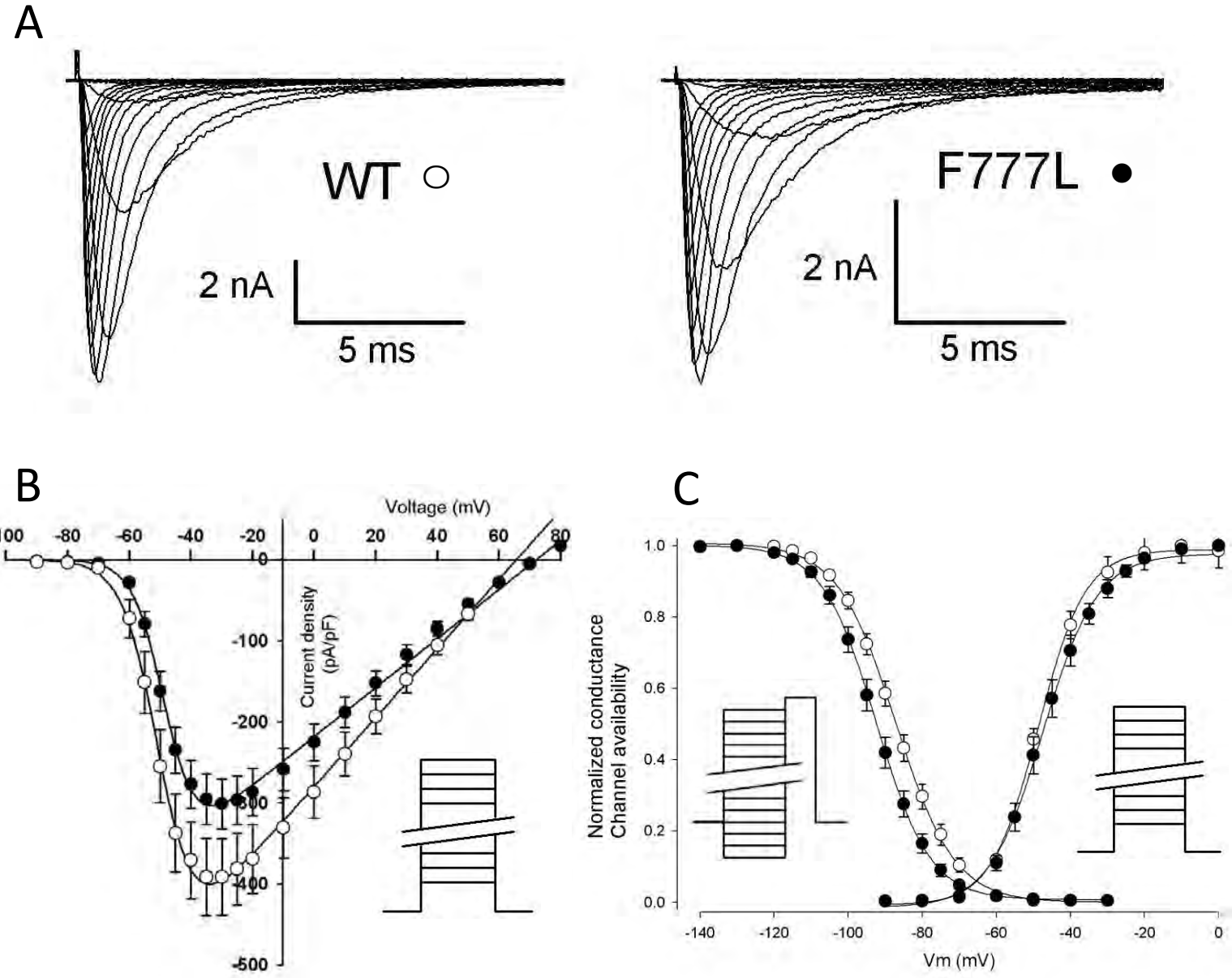
A
WT ○
2 nA
5 ms
F777L ●
2 nA
5 ms
B
Voltage (mV)
-100 -80 -60 -40 -20 0 20 40 60 80
0
-100
-200
-300
-400
-500
Current density (pA/pF)
C
Normalized conductance
Channel availability
1.0
0.8
0.6
0.4
0.2
0.0
-140 -120 -100 -80 -60 -40 -20 0
Vm (mV)

VT initiation at 1’17” (recovery phase)

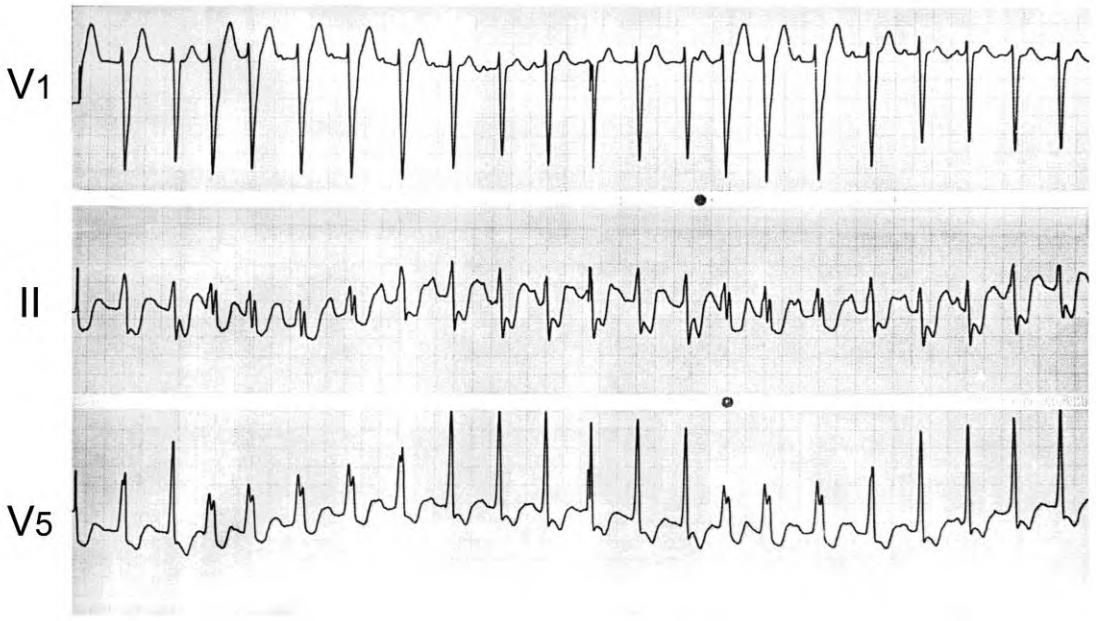

Spontaneous VT termination at 20’23”

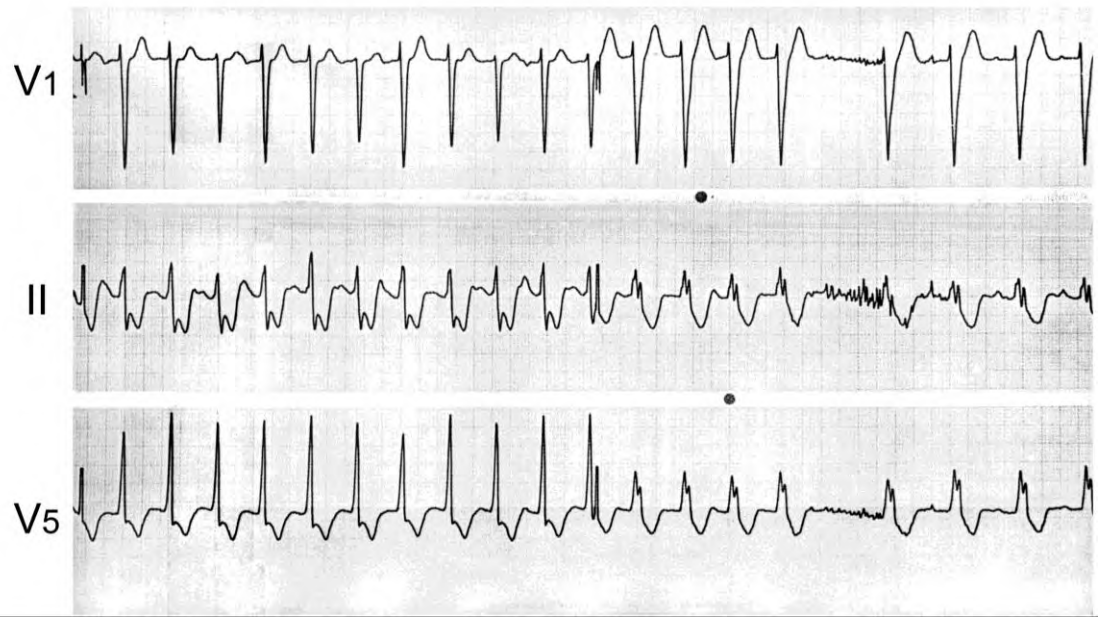

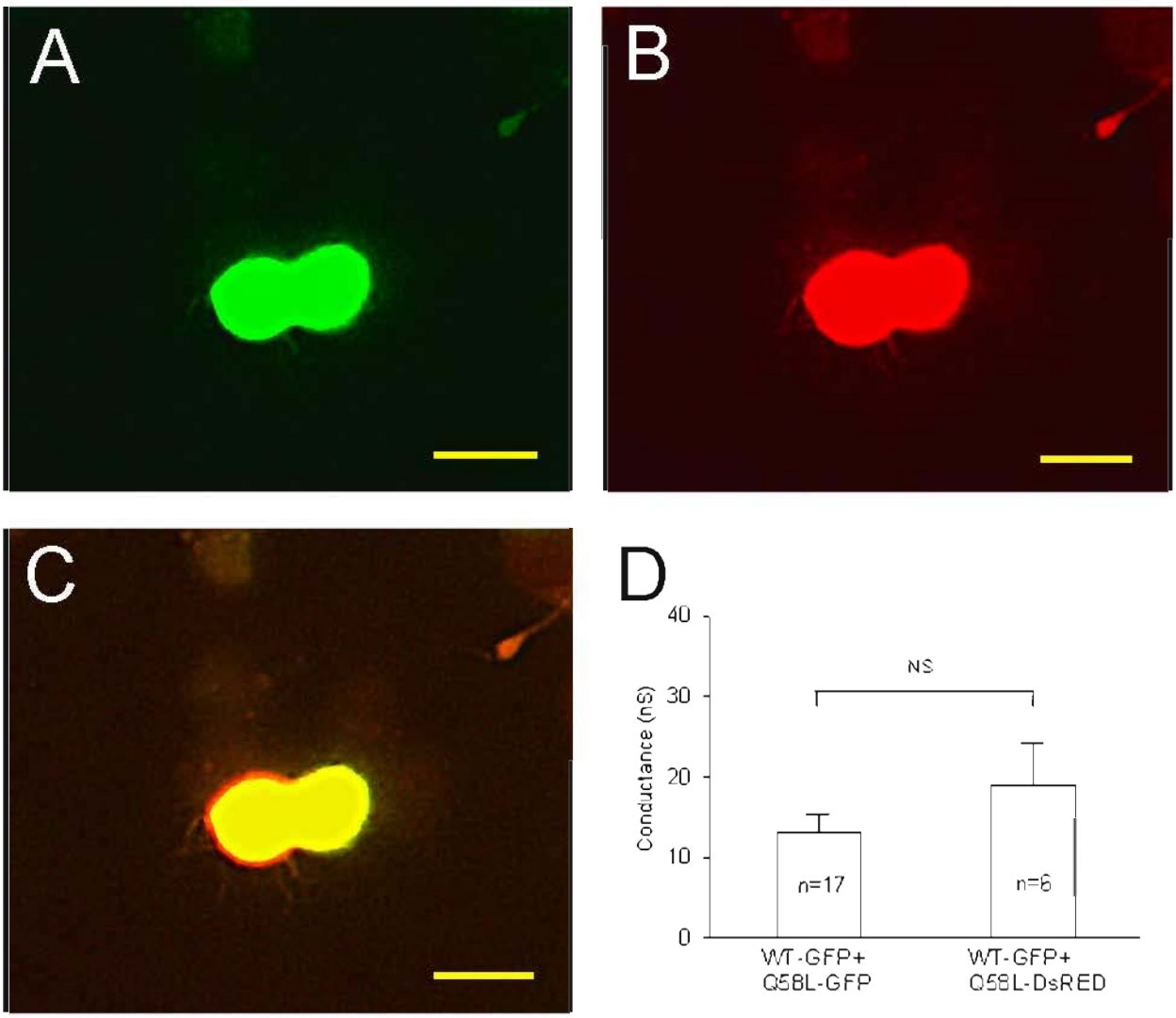
A
B
C
D
40
30
20
10
0
Conductance (nS)
NS
n=17
n=6
WT-GFP+
Q58L-GFP
WT-GFP+
Q58L-DsRED

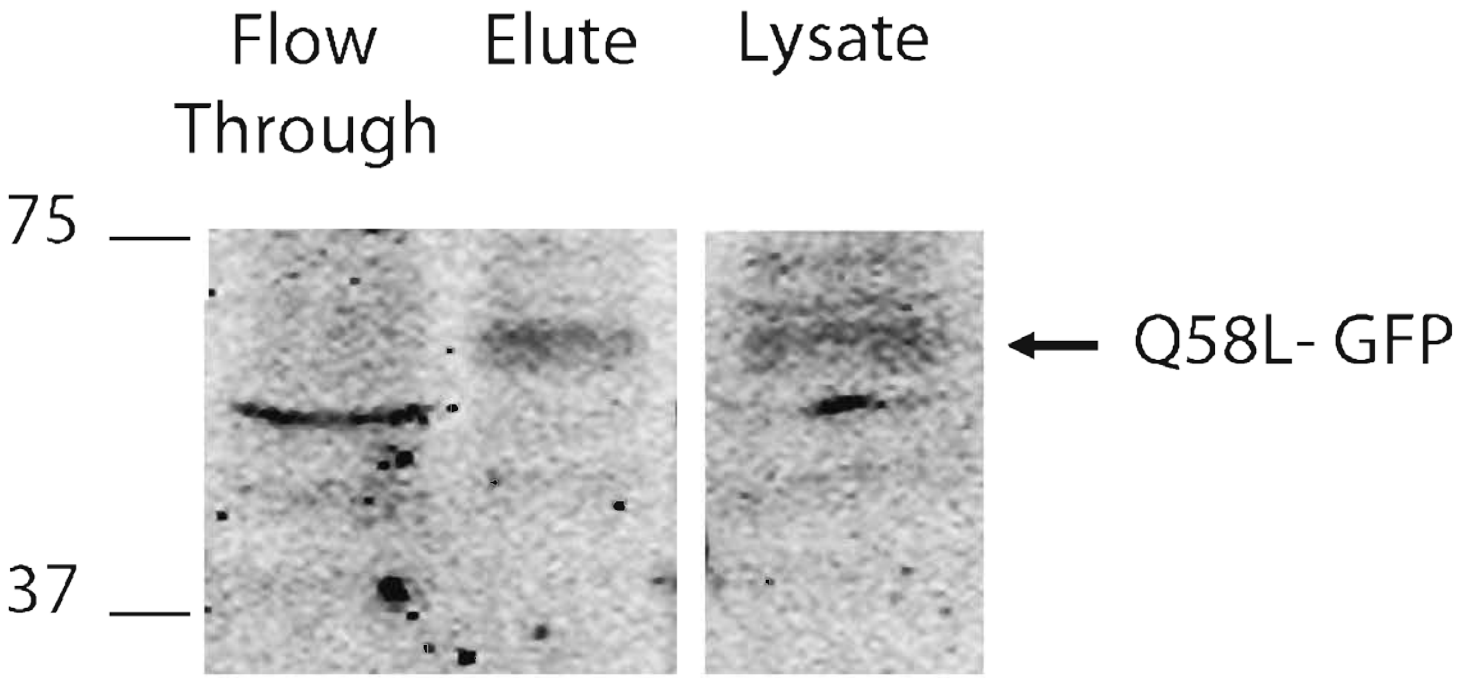
Flow Through
Elute
Lysate
75
37
Q58L- GFP

Supplemental Table S1. Genetic mutations identified in PFHBI probands

Patient	Gene	Exon	cDNA mutation	Amino acid change	Mutation type	Phenotype	Reference
1 †	*GJA5*	2	c.173 A>T	Q58L	Missense	PFHBI	this study
2	*SCN5A*	15	c.2329T>C	F777L	Missense	PFHBI +DCM+MMD	this study
3 †*	*SCN5A*	14	c.2102 del C	p.P701fsX710	Deletion	PFHBI +BrS	this study
	SCN5A	28	c.6017 delC	p.P2006fsX2037	Deletion		this study
4	*SCN5A*	28	c.5290 delG	p.V1764fsX1786	Deletion	PFHBI +BrS+MMD	this study
5	*SCN5A*	20	c.3539C>T	A1180V	Missense	PFHBI +DCM	[11]
6	*SCN5A*	21	c. 3823G>A	D1275N	Missense	PFHBI +DCM	[12]
7	*SCN5A*	Int22	IVS22+2T>C		Exon skipping	PFHBI	[13]
8	*SCN5A*	28	c.5280 delG	p.A1711fsX1786	Deletion	PFHBI	[13]
9	*SCN5A*	28	c. 5129C>T	S1710L	Missense	PFHBI +IVF	[14]
10	*SCN1B*	3	c.259G>C	E87Q	Missense	PFHBI	[5]
11	*SCN1B*	3A	c.536G>A	W179X	Missense	PFHBI+BrS	[5]
12	*SCN1B*	3A	c.537G>A	W179X	Missense	PFHBI	[5]

GJA5: connexin 40, *SCN5A*: cardiac voltage-gated Na channel α subunit, *SCN1B*: voltage-gated Na channel β1 subunit

†: Patients 1 and 3 are sudden cardiac death victims

*: Patient 3 is a compound heterozygous carrier of *SCN5A* mutations

DCM: dilated cardiomyopathy, MMD: myotonic muscular dystrophy, BrS: Brugada syndrome, IVF: idiopathic ventricular fibrillation, Int22: Intron 22

Supplemental Table S2. ECG parameters of the family members

Family	Age	HR (bpm)	PR (ms)	QRS (ms)	QTc (ms)	Axis (degree)	ST depression
Proband	6	87	*	126	421	-8	II,III,aVF, V3-6
	8	77	*	128	396	-21	II,III,aVF, V2-6
Sister	6	86	130	86	404	-25	II,III,aVF, V3-6
	11	85	142	88	416	-49	II,III,aVF, V3-6
Mother	16	63	248	152	471	-25	II,III,aVF, V3-6

*: advanced AV block